



# The Feedback Loop in Impinging Two-Dimensional High-Subsonic and Supersonic Jets

**K. Hourigan**

**M. Rudman**

*Commonwealth Scientific and Industrial Research Organisation, Division of Building, Construction and Engineering, Highett, Victoria, Australia*

**E. Brocher**

*Institut de Mécanique des Fluides, Université d'Aix-Marseille, U.M. 34 of the C.N.R.S., Marseille, France*

■ The instabilities in a supersonic impinging jet are investigated by solving the two-dimensional Euler equations using the piecewise parabolic method (PPM) and Roe's linearized Riemann solver. The predicted shock cell spacing agrees well with the observed and theoretical values. The frequency and nature of the dominant instabilities are found to be a function of the impingement distance. Two instability modes are possible: a symmetric (or varicose) mode and an asymmetric (or sinuous) mode. For two given jet exit Mach numbers ( $M = 0.98$  and  $1.29$ ), the energy in, and frequency of, these modes are functions of impingement distance, leading to an integral staging due to an acoustic feedback loop. The predicted frequencies of the fundamental symmetric and asymmetric instabilities agree with the theoretically allowed values. The staging of predicted frequencies that occurs in experimental work is also predicted.

**Keywords:** *acoustic feedback loop, impinging jet, staging*

## INTRODUCTION

Below a jet Mach number of 0.6, no tones are observed for cold jets impinging normally to a wall. The strong tones emitted when high-subsonic or supersonic jets impinge normal to a wall have been found to contain frequency jumps as the distance to the wall is varied gradually [1, 2]. This staging effect is characteristic of systems driven by acoustic feedback. For round impinging subsonic jets, Neuwerth identified the feedback acoustic disturbances inside the jet column through analysis of high-speed movies. Ho and Nossier [3] investigated the feedback loop and the associated acoustic tones for subsonic impinging jets.

In round jets, the allowable frequencies of the helical neutral wave modes that propagate upstream are too high to match those of the instability waves of the jet at subsonic Mach numbers. At supersonic Mach numbers, frequency matching becomes possible; the stable helical feedback loop and the generation of impingement tones can be maintained. Tam and Ahuja [4] proposed that the feedback was achieved by a family of upstream propagating acoustic waves of the jet flow (see Fig. 1). For subsonic jets, these waves can exist inside the jet; for the supersonic case, the acoustic waves are restricted to traveling upstream outside of the jet. In the subsonic case, the instability waves in the jet were invariably axisymmetric, whereas in the supersonic case both axisymmetric and

helical modes were observed. Tam and Ahuja were able to predict the average impingement tone frequency at different jet Mach numbers and also explain why no tones were observed for cold jets for Mach numbers less than 0.6.

In supersonic rectangular jets, although the noise spectrum consists of many tones, there are only two basic tone frequencies [5]. The basic frequency associated with an antisymmetric mode is higher than the basic tone associated with a symmetric mode. All of the other tones in the spectrum are found to be combination tones of the two basic tones and their harmonics and are generated by the nonlinearities of the jet flow.

In this paper, we model the impingement process for a supersonic two-dimensional impinging jet, using the piecewise parabolic method, with the aim of understanding the mechanisms involved in the feedback process.

## NUMERICAL METHOD

The two-dimensional Euler equations for compressible hydrodynamics are written in conservation form. For Cartesian ( $x, y$ ) coordinates they are

$$\frac{\partial U}{\partial t} + \frac{\partial F(U)}{\partial x} + \frac{\partial G(U)}{\partial y} = 0, \quad (1)$$

Address correspondence to Dr. M. Rudman, CSIRO Division of Building, Construction and Engineering, P.O. Box 56, Highett 3190, Australia.

*Experimental Thermal and Fluid Science* 1996; 12:265–270

© Commonwealth Scientific and Industrial Research Organisation (CSIRO), 1996

Published by Elsevier Science Inc., 1996

655 Avenue of the Americas, New York, NY 10010

0894-1777/96/\$0.00  
SSDI 0894-1777(95)00084-4

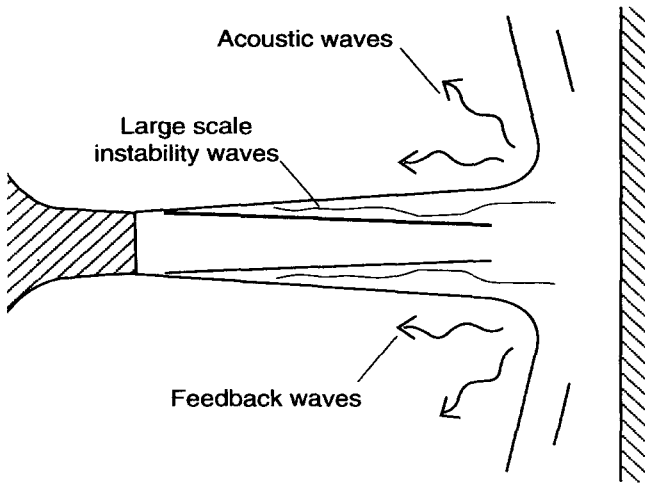


Figure 1. Schematic of the feedback loop of an impinging jet.

where

$$U = \begin{pmatrix} \rho \\ \rho u \\ \rho v \\ \rho E \end{pmatrix}, \quad F(U) = \begin{pmatrix} \rho u \\ \rho u^2 + p \\ \rho uv \\ (\rho E + p)u \end{pmatrix}, \quad (2)$$

$$G(U) = \begin{pmatrix} \rho v \\ \rho uv \\ \rho v^2 + p \\ (\rho E + p)v \end{pmatrix}.$$

Equation (1) is solved by using a PPM scheme. The PPM scheme is a characteristic-based method and a higher order extension of Godunov's method [6] as developed by Colella and Woodward [7]. The code used here is due to Gathmann [8]. The multidimensional problem posed in Eq. (1) is approached using direction splitting, with the problem decomposed into two one-dimensional hyperbolic problems:

$$L_x(U) = 0 \quad \text{and} \quad L_y(U) = 0, \quad (3)$$

where

$$L_x(U) = \frac{\partial U}{\partial t} + \frac{\partial F(U)}{\partial x} \quad \text{and}$$

$$L_y(U) = \frac{\partial U}{\partial t} + \frac{\partial G(U)}{\partial y}. \quad (4)$$

The solution at time level  $n + 2$  is determined as follows:

$$U^{n+2} = L_y L_x L_x L_y(U^n). \quad (5)$$

The PPM algorithm defines a piecewise interpolation function for each primitive variable  $v_i \in \{\rho, u, v, p\}$  that is parabolic over each cell. The piecewise parabolic interpolation is modified in any cell in which it would generate new extrema and is replaced near contact discontinuities with a piecewise linear distribution. This procedure ensures monotonicity of the interpolation, accuracy of shock resolution, and stability and robustness of the algorithm.

Once interpolation functions have been determined, flow variables are decomposed into three linearized  $(x, t)$  wave characteristics corresponding to upstream traveling pressure waves (where allowed), downstream traveling pressure waves, and convective transport by the flow. The decomposition is written in terms of the amplitudes and eigenvectors of the linear waves, and Roe's [9] linearized Riemann solver is applied to the state vector of conservative variables. Finally, the conservative fluxes are determined and applied. The scheme is fourth-order in time and in space where the solution is smooth, and second-order in space and third-order in time near discontinuities.

### Boundary Conditions

**Inflow** All flow variables are specified at the inflow boundaries. For the jet, the inflow velocity profile is the basic jet velocity profile investigated by Michalke [10], [11] and others and shown to match well the potential core region of a jet by Moore [12]. The profile is given by

$$u(y) = \frac{V_1}{2} \left\{ 1 - \tanh \left[ 6.25 \left( \frac{|y|}{d} + \frac{d}{|y|} \right) \right] \right\}, \quad (6)$$

where  $V_1$  is the speed at the center of the jet at exit and  $d$  is the jet width. Using the formula derived by Crighton and Gaster [13] for zero external flow, the momentum thickness  $\theta$  of the jet shear layer at axial position  $x$  downstream of the jet exit is given by  $d/\theta = 100/(3x/d + 2)$ , giving an initial thickness of  $\theta/d = 0.02$ .

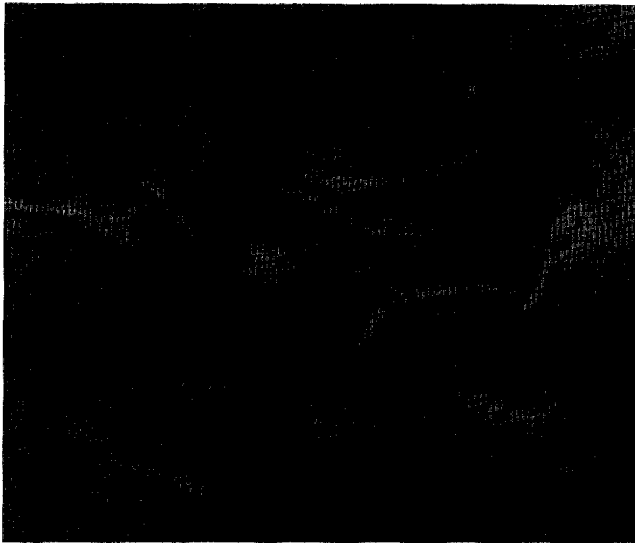
**Outflow** All  $(x, t)$  characteristics are directed outward, and the flow depends neither physically nor numerically on the outflow boundary values. The boundary condition for the pressure represents a radiation condition. Negligible reflection was detected in the simulations.

**Grid** As discussed in the next section, a fine uniform grid of size  $256 \times 128$  was finally used for each simulation. Typically the grid spacing in the transverse direction was comparable to the initial jet shear layer thickness and sufficiently fine to capture the development of the shear layer instabilities.

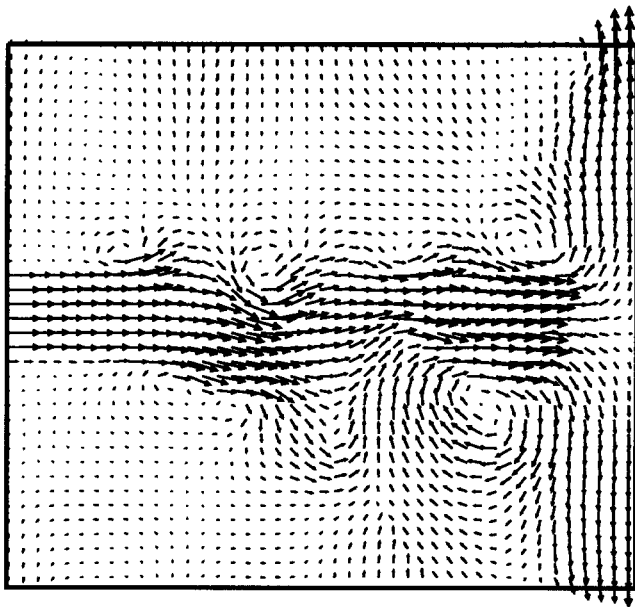
## RESULTS AND DISCUSSION

The code has been used to model the time-dependent impinging jet over a range of impingement distances for both a subsonic and a supersonic jet of exit Mach numbers 0.98 and 1.29. A key requirement in the simulations is ensuring that grid resolution is high enough to capture the smallest scales of motion involved in the feedback loop. The code was tested for sensitivity of the predicted frequencies of jet instabilities for a number of grid resolutions for the  $M_1 = 1.29$  case. Increasing from a grid size of  $128 \times 64$  to  $256 \times 128$ , the major spike in the spectra remained at the same frequency (increasing only slightly in energy), indicating that satisfactory resolution had been achieved. For a smaller grid of  $64 \times 32$ , the higher frequency spike had relatively small energy, indicating lack of resolution. The largest grid is used in all of the results presented here.

For the supersonic case, the predicted instantaneous flow for the impingement distance  $h/d = 7.0$  is shown in



**Figure 2.** (a) Plot of predicted instantaneous flow (Schlieren representation) at impingement distance of  $h/d = 7.0$  (flow entering from left,  $M_1 = 1.29$ ).



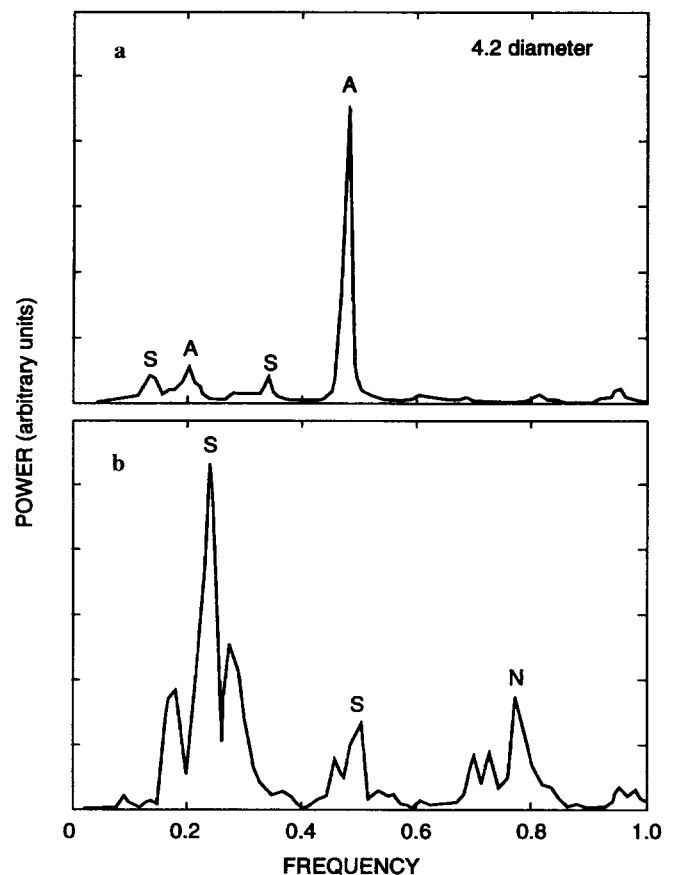
**Figure 2.** (b) Plot of predicted instantaneous velocity vectors at impingement distance of  $h/d = 6.0$ . Flow entering from left, only every third vector in each direction plotted, same instant as Fig. 2a,  $M_1 = 1.29$ .

Fig. 2 in the form of a pseudo-Schlieren plot and a velocity vector field. The code has captured weak shock cells near the jet exit. The (weak) shock cell length  $L$  of approximately 1.6 jet widths is consistent with the theoretical value from the linear analysis of Tam [14], that is,  $L = 2(M_1^2 - 1)^{1/2}d = 1.6$  for  $M_1 = 1.29$ , and that observed by Norum [15]. Sound waves are seen emanating from the impingement region. The large-scale instabilities in the jet are also prominent. Analyzing the videotape recordings of these simulations, the sound waves travel

outside the jet and interact with the shear layers near the jet exit, as postulated by Tam and Ahuja [4]. New instabilities are triggered by the sound waves near the jet exit, convect toward the wall, and generate sound waves to complete the feedback loop.

The power spectra for different impingement distances for the two different Mach number cases are shown in Figs. 3–6. In both cases, the frequency and magnitude of the dominant peaks are a function of the impingement distance. Two numerical probes were used to measure the pressure fluctuations on each side of the jet exit. The transfer function enabled the distinction between symmetric and asymmetric modes, which are denoted in Figs. 3–6. The number of impingement tones and their amplitudes and frequencies are clearly a function of the impingement distance as well as the Mach number.

In terms of a simple feedback model, the feedback loop consists of acoustic waves traveling outside the jet at the ambient speed of sound,  $a$ , and triggering, at the receptive nozzle exit, jet instabilities that convect downstream with mean velocity  $V_c = aV_L$ . The half-length of the feedback loop is the impingement distance  $h$ . The loop Strouhal number,  $St_L$ , is defined as  $fh/V_L$ , where  $V_L = V_c/(1 + V_c/a)$  is the loop velocity. When the feedback loop is operating, there will be an integral number,  $n$ , of waves in the feedback loop, that is,  $St_L = n$ .



**Figure 3.** Power spectra (arbitrary units) for impingement distance  $h/d = 4.2$ . (a)  $M_1 = 1.29$ ; (b)  $M_1 = 0.98$ . A, Asymmetric mode; S, symmetric mode; N, a mode whose phase is not distinctly asymmetric or symmetric.

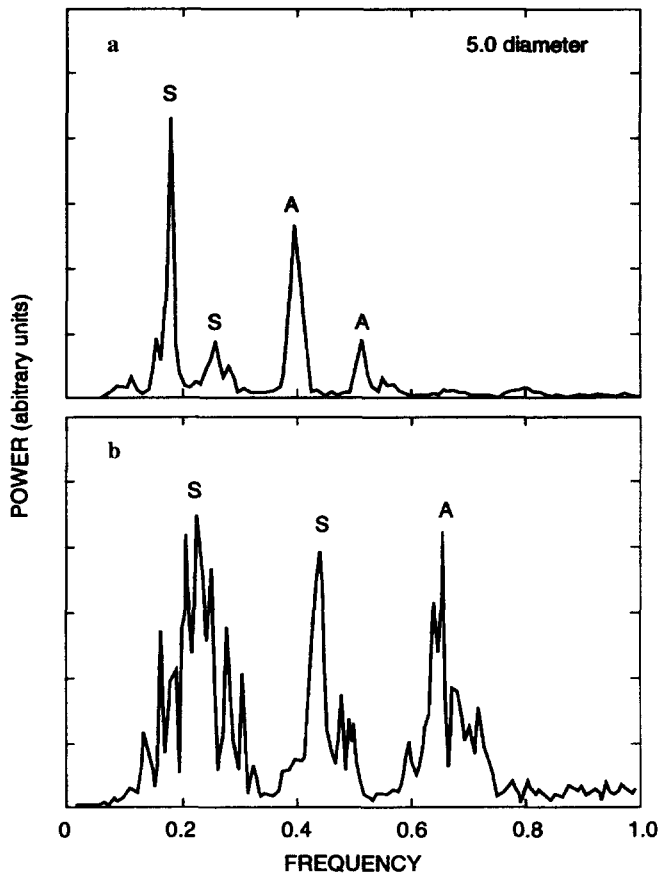


**Figure 4.** Power spectra (arbitrary units) for impingement distance  $h/d = 5.0$ . (a)  $M_1 = 1.29$ ; (b)  $M_1 = 0.98$ . A, S, N defined as in Fig. 3.

In Fig. 7, plots of the loop Strouhal number variation of the strongest tones with impingement distance for the two Mach numbers are shown. Here, best fit is obtained for  $a = 0.58$ , which is in the range 0.53–0.62 used by other researchers. The symbols indicate the relative magnitude of the spectral peaks for each impingement distance. Staging of the impingement tones (generally into integral values) of the loop Strouhal number is observed, reinforcing the theory that a feedback loop is operating for both the subsonic and supersonic cases.

For each impingement distance, the predicted lowest frequency impingement tone is due to a symmetric mode. This is in line with the theoretical analysis of Tam and Norum [5], who determined that the first symmetric mode was always lower in frequency than the first asymmetric mode, as observed in their experiments.

The results of the numerical model are in agreement with the theoretical analysis of Tam [14] and show the staging effect observed by Norum [15]. Differences arise due to the presence of strong shocks in the experiments, leading to the significant influence of the screech tone. Further differences in the selected frequency could arise from nozzle tip geometry and convergence angle. The initial set of results presented here indicates that the code is capable of providing useful insights into the coupling of impingement tones and jet instabilities. It is intended that the study be extended in the future to test the sensitivity

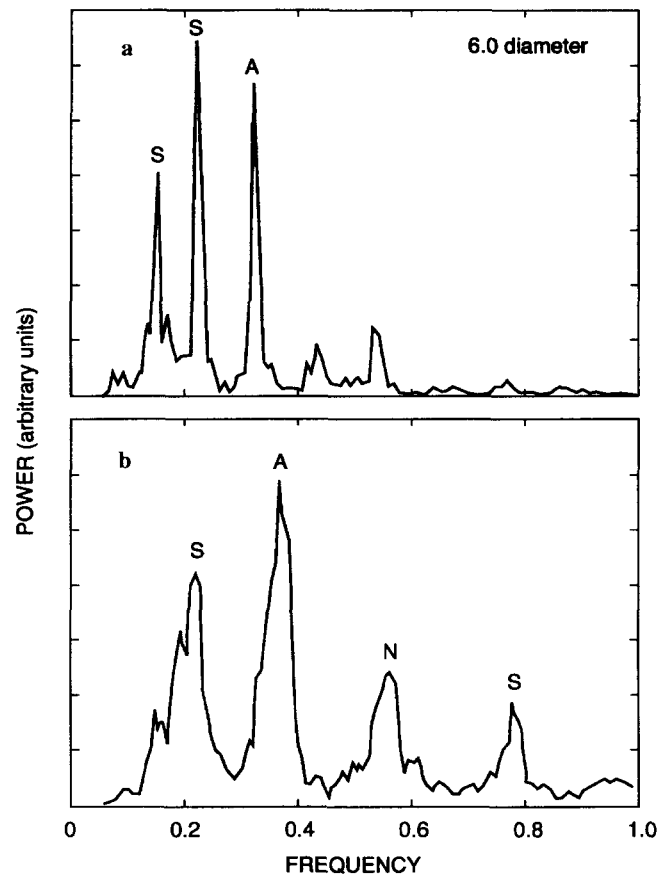


**Figure 5.** Power spectra (arbitrary units) for impingement distance  $h/d = 6.0$ . (a)  $M_1 = 1.29$ ; (b)  $M_1 = 0.98$ . A, S, N defined in Fig. 3.

of the selected impingement frequencies on nozzle shape and convergence angles over a wider range of impingement distances and different jet exit Mach numbers.

### PRACTICAL SIGNIFICANCE

Impinging jets are commonplace in industrial applications, including mixing and spraying, where flow steadiness is desirable. In the aerospace industry, rocket launches represent a critical phase during which jet instabilities can lead to payload damage and loss of flight control. The present study seeks to understand the mechanisms leading to the appearance of instabilities in impinging jets. In the longer term, it is hoped that flow control guidelines will emerge from these types of studies.

### CONCLUSIONS

The existence of acoustic feedback loops, as postulated previously from experiments, in impinging supersonic jets has been demonstrated using a high-order numerical method. The Strouhal number associated with the impingement tones is found to be generally integral when normalized with respect to the loop velocity and impingement distance. The feedback loop consists of the generation of acoustic waves near impingement that travel upstream and excite the jet modes in the receptive region

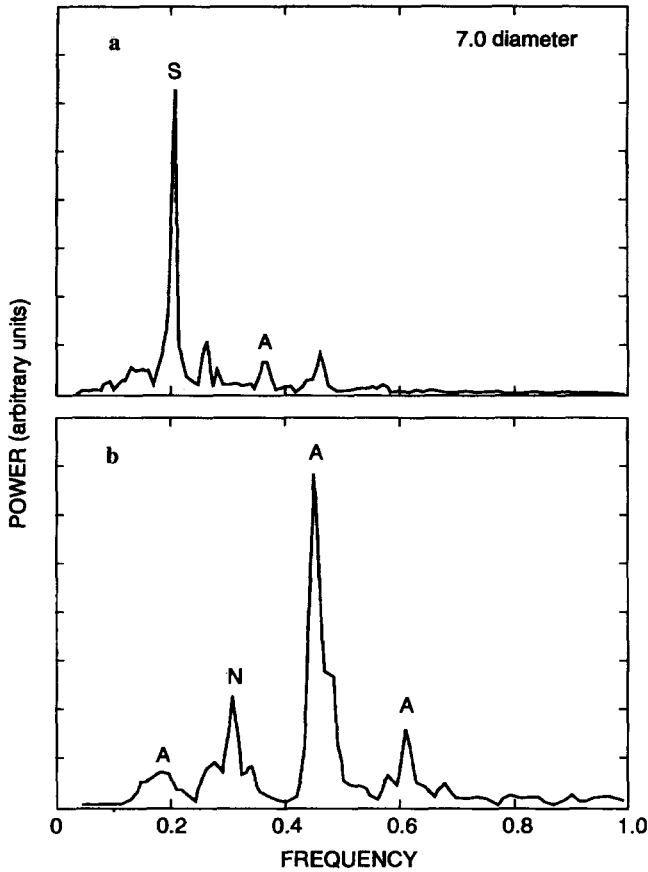


**Figure 6.** Power spectra (arbitrary units) for impingement distance  $h/d = 7.0$ . (a)  $M_1 = 1.29$ ; (b)  $M_1 = 0.98$ . A, S, N defined as in Fig. 3.

near the jet outlet. The jet instabilities then convect toward the wall and generate acoustic waves upon impingement. Depending on the impingement distance, both symmetric and asymmetric jet instability modes may be present, as observed experimentally.

It is intended to broaden the study by considering different Mach number jet flows and comparing the results with those obtained using a hydraulic analogy.

We thank Dr. Ralf Gathmann for providing the basic PPM code used for the numerical simulation. Dr. Rudman gratefully acknowledges the assistance of a CSIRO Postdoctoral Award. Dr. Hourigan gratefully acknowledges the support of the CNRS of France and DIST of Australia.

#### NOMENCLATURE

- $a$  ambient sound speed, m/s  
 $a$  ratio of convection to jet exit velocities, dimensionless  
 $d$  jet nozzle width, m  
 $E$  total energy per unit mass, J/kg  
 $e$  internal energy per unit mass [ $= E - 1/2(u^2 + v^2)$ ], J/kg  
 $F$  nonlinear flux operator in the  $x$  direction, kg m/s, N/m<sup>2</sup>, N/m<sup>2</sup>, N/ms

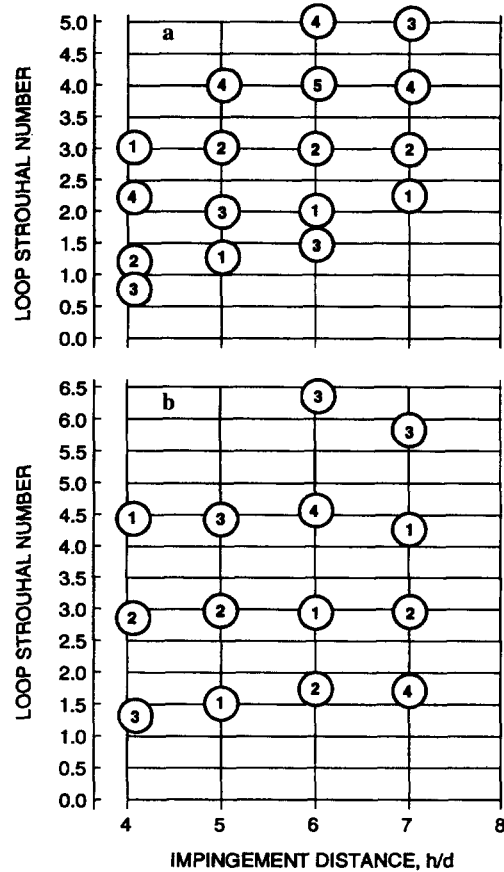


**Figure 7.** Loop Strouhal number  $St_L$  of the loudest tones versus impingement distance  $h/d$  for (a)  $M_1 = 1.29$  and (b)  $M_1 = 0.98$ . The numbers in the circles indicate decreasing magnitude of tones for each impingement distance (1 = largest magnitude, etc.).

- $f$  frequency of impingement tone, Hz  
 $G$  nonlinear flux operator in the  $y$  direction, kg m/s, N/m<sup>2</sup>, N/m<sup>2</sup>, N/ms  
 $h$  distance between nozzle and wall, m  
 $L$  shock cell length, m  
 $L_x$  operator of the Euler equation solution in the  $x$  direction, dimensionless  
 $L_y$  operator of the Euler equation solution in the  $y$  direction, dimensionless  
 $M_1$  jet exit Mach number, dimensionless  
 $n$  number of periods of sound wave in feedback loop, dimensionless  
 $p$  pressure, Pa  
 $r$  local fluid density, kg/m<sup>3</sup>  
 $St_L$  loop Strouhal number [ $= fh/V_L$ ], dimensionless  
 $t$  time, s  
 $U$  state vector of the flow, kg/m<sup>3</sup>, kg/m<sup>2</sup>/s, kg/m<sup>2</sup>/s, J/m<sup>3</sup>  
 $u$  velocity in the axial  $x$  direction, m/s  
 $V_c$  average convection velocity, m/s  
 $V_L$  loop velocity [ $= V_c/(1 + V_c/a)$ ], m/s  
 $V_1$  jet exit velocity, m/s  
 $v$  velocity in the transverse direction, m/s

- $v_i$  interpolation function of the primitive variables,  
 $\text{kg/m}^3$ ,  $\text{m/s}$ ,  $\text{m/s}$ ,  $\text{Pa}$   
 $x$  axial distance,  $\text{m}$   
 $y$  transverse distance,  $\text{m}$

**Greek Symbol**

- $\theta$  momentum thickness of the jet shear layer,  $\text{m}$

**REFERENCES**

1. Wagner, F. R., The Sound and Flow Field of an Axially Symmetric Free Jet upon Impact on a Wall, NASA TT F-13942, 1971.
2. Neuwerth, G., Acoustic Feedback of a Subsonic and Supersonic Free Jet Which Impinge on an Obstacle, NASA TT F-15719, 1974.
3. Ho, C. M., and Nossier, N. S., Dynamics of an Impinging Jet. Part I. The Feedback Phenomenon, *J. Fluid Mech.* **105**, 119–142, 1981.
4. Tam, C. K. W., and Ahuja, K. K., Theoretical Model of Discrete Tone Generation by Impinging Jets, *J. Fluid Mech.* **214**, 67–87, 1990.
5. Tam, C. K. W., and Norum, T. D., Impingement Tones of Large Aspect Ratio Supersonic Jets, *AIAA J.* **30**, 304–311, 1992.
6. Godunov, S. K., Difference Methods for Numerical Calculation of the Equations of Fluid Dynamics, *Math. Sb.* **47**, 271–306, 1959.
7. Colella, P., and Woodward, P. R., The Piecewise Parabolic Method (PPM) for Gas-Dynamical Simulations, *J. Comp. Phys.* **54**, 174–201, 1984.
8. Gathmann, R., Analyse d'écoulements supersoniques et reactifs par simulation numerique instationnaire tridimensionnelle, Ph.D. thesis, Institut de Mecanique de Grenoble, 1993.
9. Roe, P. L., Approximate Riemann Solvers, Parameter Vectors and Difference Schemes, *J. Comp. Phys.* **43**, 357–372, 1981.
10. Michalke, A., Instability of Compressible Circular Free Jet with Consideration of the Influence of the Jet Boundary Layer Thickness, NASA Tech. Memo. 75190, 1977.
11. Michalke, A., and Hermann, G., On the Inviscid Instability of a Circular Jet with External Flow, *J. Fluid Mech.* **114**, 343–359, 1982.
12. Moore, C. J., The Role of Shear-Layer Instability Waves in Jet Exhaust Noise, *J. Fluid Mech.* **77**, 511–529, 1976.
13. Crighton, D. G., and Gaster, M., Stability of Slowly Diverging Jet Flow, *J. Fluid Mech.* **77**, 397–413, 1976.
14. Tam, C. K. W., The Shock-Cell Structures and Screech Tone Frequencies of Rectangular and Non-Axisymmetric Supersonic Jets, *J. Sound Vibration* **121**(1), 135–147, 1988.
15. Norum, T. D., Supersonic Rectangular Jet Impingement Noise Experiments, AIAA Paper No. 89-1138, 1–12, 1989.

---

Accepted August 24, 1995